

JI-HYUN YOON<sup>1\*</sup>, JEOUNG HAN KIM<sup>2</sup>

## CHARACTERISTICS OF 3D PRINTED FUNCTIONALLY GRADED MATERIAL FOR REPLACEMENT OF DISSIMILAR METAL WELD IN NUCLEAR REACTOR

The dissimilar metal welds in the most of the reactors are connections between low alloy steel parts and stainless steel piping. There is a high possibility of primary water stress corrosion cracking (PWSCC) damage attributed to residual stress caused by the difference in material properties in the dissimilar metal weld joints. A number of accidents such as leakage of radioactive coolant due to PWSCC have been reported around the world, posing a great threat to nuclear safety. The objective of this study is to develop a technology that can fundamentally remove dissimilar metal welds by replacing the existing dissimilar metal parts with the functionally graded material (FGM) manufactured by metal 3D printing consisting of low alloy steel and austenitic stainless steel. A powder production, mixing ratio calculation, and metal 3D printing were performed to fabricate the low alloy steel-stainless steel FGM, and microstructure analysis, mechanical properties, and coefficient of thermal expansion (CTE) measurement of the FGM were performed. As a result, it is observed that CTE tended to increase as the austenite content increased in FGM. The gradual change of coefficient of thermal expansion in a FGM showed that the additive manufacturing using 3D printing was effective for preventing an abrupt change in thermal expansion properties throughout their layers.

**Keywords:** Functionally Graded Material (FGM); PWSCC; 3D Printing; Reactor; Coefficient of Thermal Expansion (CTE)

### 1. Introduction

Since various parts of a nuclear reactor are manufactured with different steel types depending on the purpose of use and environment, dissimilar metal welds are used in nuclear power plants at locations where two different types of materials, e.g., low alloy steel and stainless steel are joined. The nickel-base alloy dissimilar metal welds are typically made of Alloy 182 and Alloy 82 equivalent to Alloy 600 to accommodate the differences in composition and thermal expansion of the two alloys.

When welding dissimilar materials, the resulting residual stress state is further influenced by the mismatch in adjoining material properties in comparison to welding materials of the same type. By virtue of the imbalance in mechanical and thermal properties of the adjoining materials, a complex intrinsic stress state is induced. This residual stress component is added to those related to the welding procedure.

There is a high possibility of PWSCC damage attributed to residual stress caused by the difference in material properties in the dissimilar metal weld joints. A number of accidents such as

leakage of radioactive coolant due to PWSCC have been reported around the world, posing a great threat to nuclear safety [1].

From the previous experiences of PWSCC of Alloy 600 components in primary water reactor (PWR) [1], thin-wall tubing and thick-wall piping have been made from the higher Cr-containing Alloy 690 in the last several decades [2]. Until now, there have been no reports of corrosion cracking failures of components made from Alloy 690 in operating PWRs. However, it has been recently reported that Alloy 690 is also susceptible to PWSCC in certain experimental conditions, especially when work-hardened [3-5] by welding, machining or surface finishing during the fabrication or field repair of the components.

Although alloy 52/152 is superior to alloy 82/182 in terms of corrosion resistance, but due to the limitation of an austenitic alloy, when used as a welding material between ferritic steel and austenitic stainless steel, there is still a mismatch in thermo-mechanical properties resulting from a sharp difference in coefficient of thermal expansion (CTE).

As international competition for leadership in the era of the 4th industrial revolution intensifies, significant advancements

<sup>1</sup> KOREA ATOMIC ENERGY RESEARCH INSTITUTE, DAEJEON, SOUTH KOREA

<sup>2</sup> HANBAT NATIONAL UNIVERSITY, DAEJEON, SOUTH KOREA

\* Corresponding author: [jhyoon4@kaeri.re.kr](mailto:jhyoon4@kaeri.re.kr)



are being made in 3D printing technology, a core component of this revolution. In the nuclear industry, numerous countries, including the United States, are actively engaged in the development of nuclear-grade parts using 3D printing technology. This progress is rapidly establishing a technological environment that can enhance the safety of existing nuclear reactors by leveraging the advantages offered by 3D printed components [2,6].

The dissimilar metal welds in the most of the nuclear reactor are connections between low alloy steel parts and stainless steel piping. Therefore, we tried to develop a technology that can fundamentally remove dissimilar metal welds by replacing the existing dissimilar metal parts with the FGM manufactured by metal 3D printing consisting of low alloy steel and austenitic stainless steel. A multi-material part that is formed with at least two materials whose distribution changes with width, FGMs, whose microstructure and composition change gradually across the part could be used as a part such as safe-end for the joint between dissimilar metal parts to reduce the PWSCC as shown in Fig. 1.

## 2. Experimental

### 2.1. Procurement of Alloy Powder for 3D Printing

To fabricate a FGM in which low-alloy steel and austenitic stainless steel are additively manufactured using a 3D printer, alloy powder was prepared. The mother alloys are SA533B low alloy steel (0.21C-1.45Mn-0.54Ni-0.50Mo-0.21Si-0.21C-Fe) and Type 316L stainless steel (17.8Cr-12.8Ni-2.36Mo-0.68Si-0.019Cr-Fe), which are mainly used for pressure vessels and piping of nuclear reactors respectively. In the case of Type 316L stainless steel, commercial powder is easily available, but low alloy steel powder of the same type as that used in nuclear reactors is not available commercially. Therefore, in this study, blocks taken from SA533B low alloy steel, which is an archival material for a pressure vessel in the Kori Unit 2 nuclear reactor of South Korea, and spherical powder 45-150  $\mu\text{m}$  with an average particle size of about 100  $\mu\text{m}$ , similar to the commercial Type

316L stainless steel powder size distribution, was produced through high temperature gas atomizing.

### 2.2. Manufacturing of FGM

A direct energy deposition (DED) type 3D printer, InssTek MX-400, produced by Korean domestic company was used for 3D printing of FGM. The DED equipment uses 500 W Ytterbium fiber laser as a power source and has working envelope of 400×450×300 (mm). Under DED conditions, the output was 380-450 W, a laser beam size of 0.8 mm, the scan speed was 14.1 mm/s, a focal length of 9 mm, and the stacking was performed at a hatch interval of 400  $\mu\text{m}$  under argon gas atmosphere with a pressure of 10 mbar. The laser power was changed instantly by means of automatic feedback controlling system in DED system to maintain the layer thickness and hatch width of the deposition. A prototype was fabricated by the orthogonal scanning method, which is firstly scanned with vector along x and secondly along y starting from the same location among layers, on a 20 mm thick AISI 1045 carbon steel substrate as schematically shown in Fig. 2.

A well-shaped 5-layer FGM (100 mm-diameter, 30 mm-thickness, 35 mm-height) was manufactured using powder mixed in such a way that the fraction of ferritic phase was reduced by 25% in 4 steps from 100% to 0%. The numbers in parentheses indicate the weight % of each alloy in the powder. Layers B, C and D were each 5 mm thick, and layers A and E were 10 mm thick as shown in Fig. 3.

### 2.3. Microstructural Analysis

The elemental composition of each layer was measured by scanning electron microscopy (SEM) in conjunction with energy dispersive spectroscopy (EDS) for all elements except carbon, which was measured by inductively coupled plasma optical emission spectroscopy (ICP-OES). The ferrite content in each layer of 3D printed block was measured by using Feritscope FMP 30 (Fischer).

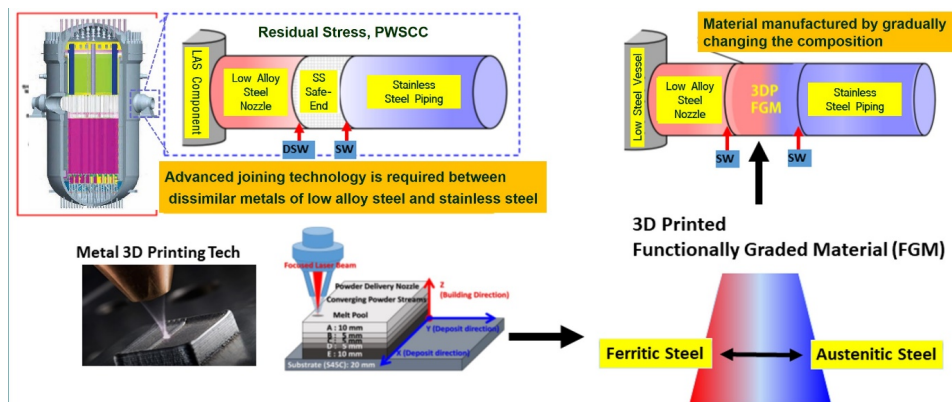


Fig. 1. Conceptual diagram of a technology that replaces the dissimilar metal welding part of a nuclear reactor with FGM produced by metal 3D printing

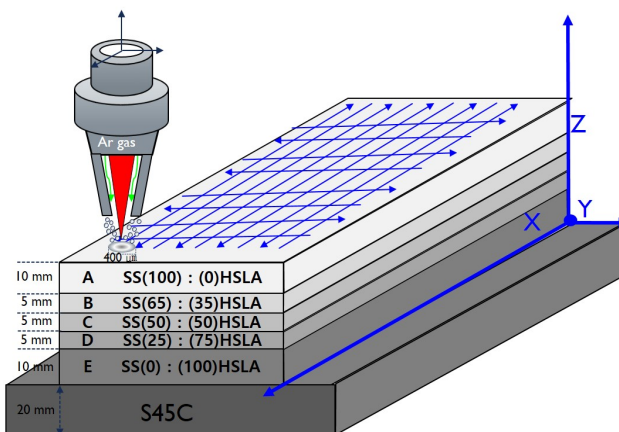


Fig. 2. Schematic of additive manufacturing process for FGM consisting of low alloy steel and austenitic stainless steel using DED type 3D printing technique

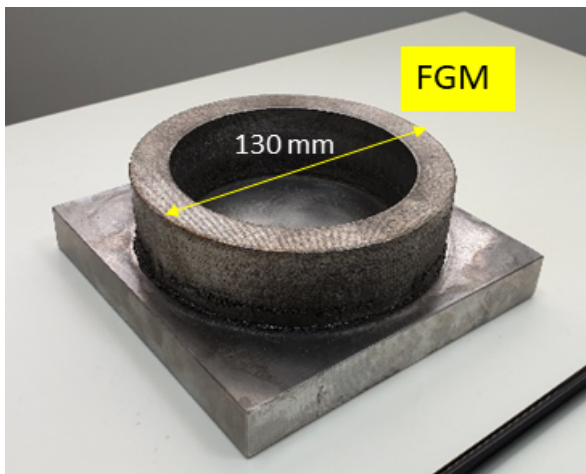


Fig. 3. Well-shaped FGM block consisting of low alloy steel and austenitic stainless steel with an outer diameter of 130 mm, thickness of 30 mm, height of 35 mm

#### 2.4. Mechanical Characterization

Tension testing was conducted for the subsize tensile specimens had a gage section of 16 mm and 2 mm thickness and were machined from the each layer of a 3D printed block for mechanical characterization. Tension testing was performed at room temperature under a strain rate of  $10^{-3}/\text{s}$  using an INSTRON-5982 servo hydraulic materials testing system in general accordance with ASTM E8/E8M-22 standard test methods [7].

#### 2.5. Thermal Expansion Measurement

The linear CTE of each layer was measured using a TMA402 F3 dilatometry system (Netzsch). The specimens were electro-discharge machined to a diameter of 4 mm and length of 25 mm. The specimens were heated from 100 to 400°C at heating rate of 5°C/min, held for 10 min, and then cooled.

### 3. Results and Discussion

#### 3.1. Microstructural characteristics

The elemental contents in layer A, which is Type 316L, through layer E, which is low alloy steel, were measured by a SEM-EDS. The compositional profiles is shown in Fig. 4. The content of Cr, Ni, and Mo decreased linearly as the ratio of low alloy steel decreased, confirming that the intended gradient composition material was obtained.

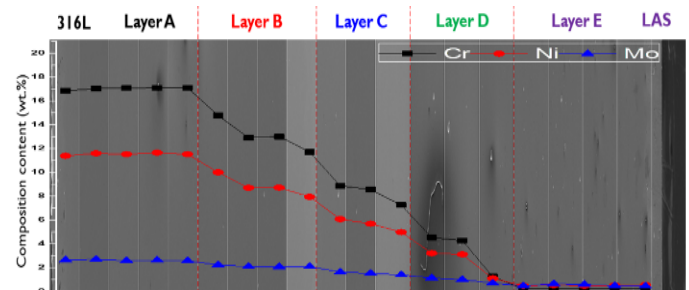


Fig. 4. Compositional profile for FGM consisting of low alloy steel and austenitic stainless steel showing gradual composition change from layer to layer

It is noteworthy that the ratios of the low alloy steel powder to the austenitic stainless powder and the fraction of ferritic phase, which was measured by magnetic method, to austenitic phase do not match. When the ratio of Type 316L stainless steel power was adjusted to 65% instead of 75% referring to the Thermo-Calc calculation results, it was possible to obtain an austenitic phase of 75% on the microstructure of 3D printed alloy [8]. The finally obtained ferrite content in each layer was almost identical to the target content.

#### 3.2. Mechanical Properties

The tensile tests for the specimens cut from each added manufactured layer the FGM block were performed in order to evaluate the mechanical properties.

As shown in Fig. 5, in the Y-direction with respect to the build-up axis, the tensile strength of layers A and B, which have a high austenite fraction, compared to layers C, D, and E, having a high ferrite fraction (655 MPa and 868 MPa, respectively) and yield strength (518 MPa and 504 MPa, respectively) were low. On the other hand, the elongation (56.5% and 82.8%, respectively) was very high. These tensile properties are attributed to work hardening that occurs in general austenitic stainless steels [9].

#### 3.3. Thermal Expansion

The uneven local thermal expansion or contraction could result in stress in a welded joint in reactor which is mainly attributed to CTE mismatches in dissimilar weld [10-11]. Thus,

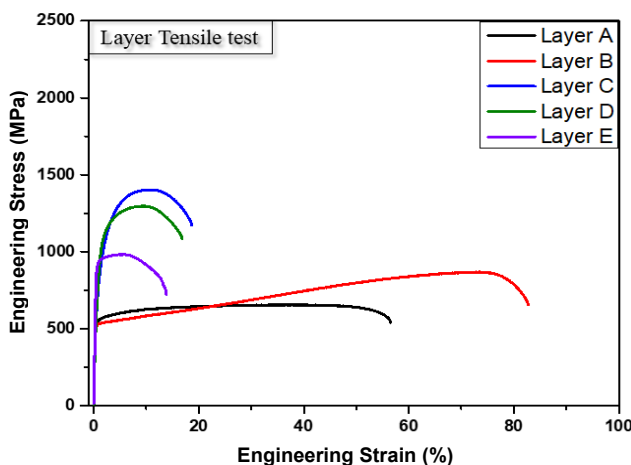


Fig. 5. Comparison of engineering stress-engineering strain curves across layers of ferrite-austenite FGM

the joining of two materials with different CTEs leads to the generation of high stress at the interface. Therefore, a graded composition over the interface can help reduce the residual stress.

The thermal expansion coefficient up to 400°C was measured for each layer of FGM using Thermomechanical Analysis (TMA). As shown in Fig. 6, CTE tended to increase as the austenite content increased.

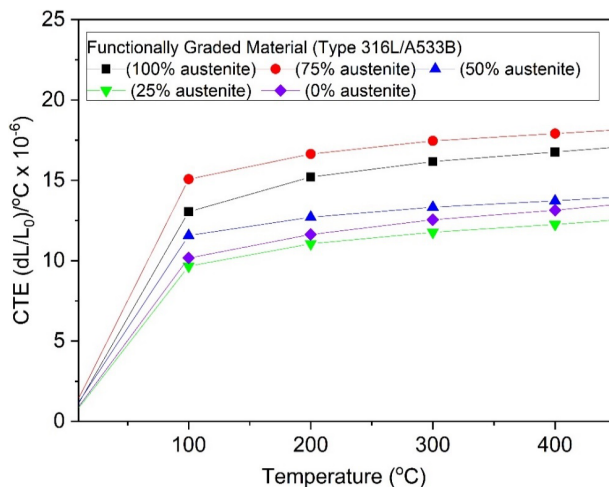


Fig. 6. Comparison of coefficient of thermal expansion (CTE) of each layer of FGM consisting of ferrite and austenite at temperature ranged 100-400°C

The gradual change of CTE values in a FGM showed that the additive manufacturing using a metal 3D printing was effective for preventing an abrupt change in thermal expansion properties throughout their layers. However it is noteworthy that layer B had much higher CTE values to ignore than layer A. It needs further investigation and to be regarded for development for industrial application.

#### 4. Conclusions

A low-alloy steel-stainless steel FGM was manufactured using 3D printing technique and characterized to prevent damage to the PWSCC of the dissimilar metal welding part of the reactor.

Powder production, mixing ratio calculation, metal 3D printing were performed to fabricate the low alloy steel-stainless steel FGM, and microstructure analysis, mechanical properties, thermal expansion coefficient measurement, and residual stress distribution analysis of the FGM were performed.

As a result, it is observed that the thermal expansion coefficient tended to increase as the austenite content increased in FGM. The gradual change of coefficient of thermal expansion in a FGM showed that the additive manufacturing using a metal 3D printing was effective for preventing an abrupt change in thermal expansion properties throughout their layers.

#### Acknowledgement

This achievement is a research conducted with the support of the National Research Foundation of Korea with funding from the Ministry of Science and ICT (NRF-2017M2A8A01 43).

#### REFERENCES

- [1] EPRI, PWSCC of Alloy 600 Type Materials in Non-Steam Generator Tubing Applications. MRP-87, Palo Alto, CA (2003).
- [2] J. Simpson, J. Haley, C. Cramer, O. Shafer, A. Elliott, W. Peter, L. Love, R. Dehoff, Considerations for Application of Additive Manufacturing to Nuclear Reactor Core Components, ORNL/TM-2019/1190, Oak Ridge, TN (2019).
- [3] P.L. Andresen, Unusual cold work and strain rate effects on SCC, in: 14<sup>th</sup> Int. Conf. On Env. Deg. Mater. Nucl. Power Syst, Water Reactors, Virginia (2009).
- [4] S.M. Bruemmer, M.J. Olszta, M.B. Toloczko, L.E. Thomas, Corrosion **69**, 953-963 (2013).
- [5] S.W. Kim, S.S. Hwang, J.M. Lee, Corrosion **71**, 1071-1081 (2015).
- [6] E.A. Kim, S.H. Kwon, D.Y. Yang, J.H. Yu, K.I. Kim, H.S. Lee, Journal of Powder Mater. **28** (3), 208-215 (2021).
- [7] ASTM International, Standard Test Methods for Tension Testing of Metallic Materials, PA, USA (2022).
- [8] J.H. Yoon et al., Development of Advanced Joining and Performance Prediction Technologies for Structural Materials of Nuclear Systems. Korea Atomic Energy Research Institute Report, KAERI/RR-4799/2021 (2021).
- [9] P. Marshall, Short-Term Mechanical Properties, Austenitic Stainless Steel: Microstructure and Mechanical Properties, New York (1984).
- [10] A. Joseph, Sanjai K. Rai, T. Jayakumar, N. Murugan, Internation Journal of Pressure Vessels and Piping **82** (9), 700-705 (2005).
- [11] M.K. Samal, M. Seidenfuss, E. Roos, K. Balani, Engineering Failure Analysis **18** (3) 999-1008 (2011).